



# Isotopic constraints on selenium degassing from basaltic magma and near-surface capture by fumarolic deposits: Implications for Se redistribution onto the Earth's surface

Carolina Rosca, Ivan Vlastélic, Maria Isabel Varas-Reus, Stephan König

## ► To cite this version:

Carolina Rosca, Ivan Vlastélic, Maria Isabel Varas-Reus, Stephan König. Isotopic constraints on selenium degassing from basaltic magma and near-surface capture by fumarolic deposits: Implications for Se redistribution onto the Earth's surface. *Chemical Geology*, 2022, 596, pp.120796. 10.1016/j.chemgeo.2022.120796 . hal-03811660

**HAL Id: hal-03811660**

**<https://uca.hal.science/hal-03811660>**

Submitted on 12 Oct 2022

**HAL** is a multi-disciplinary open access archive for the deposit and dissemination of scientific research documents, whether they are published or not. The documents may come from teaching and research institutions in France or abroad, or from public or private research centers.

L'archive ouverte pluridisciplinaire **HAL**, est destinée au dépôt et à la diffusion de documents scientifiques de niveau recherche, publiés ou non, émanant des établissements d'enseignement et de recherche français ou étrangers, des laboratoires publics ou privés.



Distributed under a Creative Commons Attribution - NonCommercial - NoDerivatives 4.0 International License

1 Isotopic constraints on selenium degassing from basaltic magma and near-surface  
2 capture by fumarolic deposits: Implications for Se redistribution onto the Earth's surface

3  
4 Carolina Rosca <sup>1\*</sup>, Ivan Vlastélic <sup>2</sup>, Maria Isabel Varas-Reus <sup>1</sup>, Stephan König <sup>1,3</sup>

5  
6 <sup>1</sup>Isotope Geochemistry Group, Dept. of Earth Sciences, University of Tuebingen,  
7 Germany

8 <sup>2</sup>Université Clermont Auvergne, CNRS, IRD, OPGC, Laboratoire Magmas et Volcans, F-  
9 63000 Clermont-Ferrand, France

10 <sup>3</sup>Instituto Andaluz de Ciencias de la Tierra (IACT), Consejo Superior de Investigaciones  
11 Científicas (CSIC) and Universidad de Granada, Avenida las Palmeras 4, Armilla, 18100  
12 Granada, Spain

13 [\\*roscaca@tcd.ie](mailto:*roscaca@tcd.ie); [carolina.rosca@uni-tuebingen.de](mailto:carolina.rosca@uni-tuebingen.de) (corresponding author)

## Abstract

Volcanic emanations from cooling basaltic lava represent a diffuse and relatively poorly constrained source of metallic and non-metallic compounds to the Earth's surface. These compounds become incorporated in fumarolic minerals and redeposit at the surface of lava flows before entering the environmental cycle. The semi-volatile and chalcophile element selenium (Se) can be either vital or toxic to animals and humans. Thus, understanding the pathways of Se capture and relative concentrations in fumaroles is imperative for estimating their contributions to soils and aquifers in volcanically active regions, with implications for animal and human health. In this study, we report Se concentrations and Se stable isotope composition in a sample suite comprising degassed and undegassed basalts and various fumarolic deposits (thenardite, Na-K sulfate, gypsum, fluoride, and native sulfur) fed from degassing lava flows at Piton de la Fournaise volcano, Réunion Island. Erupted basaltic lavas ( $136 - 58 \text{ ng}\cdot\text{g}^{-1} \text{ Se}$ ) lost up to more than half of their pre-eruptive Se due to subaerial degassing and retained a heavier isotope composition ( $\delta^{82/76}\text{Se} = 0.11 \pm 0.17 \text{ ‰}$ , 2s.d.) compared to undegassed volcanic glass ( $138 \text{ ng}\cdot\text{g}^{-1} \text{ Se}$  and  $\delta^{82/76}\text{Se} = -0.19 \pm 0.04 \text{ ‰}$ , 2s.e.). Fumarolic deposits that formed over a temperature range of  $\sim 800\text{-}100^\circ\text{C}$  and captured Se from the degassing lava show higher to very high Se concentrations ranging from  $0.54 \text{ }\mu\text{g}\cdot\text{g}^{-1}$  to  $1578 \text{ }\mu\text{g}\cdot\text{g}^{-1}$  and significant Se isotope fractionation ( $\delta^{82/76}\text{Se} = +0.6$  to  $-2.08 \text{ ‰}$ ). We propose two separate models that can explain the relative concentration and Se isotope composition of the deposits: 1) A compound oxidation state-dependent Se incorporation into the various fumarolic minerals, or 2) Temperature-dependent Rayleigh condensation from a cooling gas triggered by compound saturation. The Rayleigh condensation model can entirely explain the Se concentration and isotope composition of the fumaroles and predicts that up to 80 % of the Se released from the lava is likely to be captured by precipitation to form solid phases within the lava pile, most dramatically in the coldest deposits below the sublimation temperature of  $\text{SeO}_2$  ( $< 315^\circ\text{C}$ ). In contrast, mineral-dependent isotope pathways cannot fully explain our data, including the lighter Se isotope compositions in the more oxidized compounds compared to more reduced ones. Such a mineralogical effect cannot be excluded but further investigations and experimental studies are required in order to scrutinize and invoke its role. Finally, the environmental impact of these degassing-induced secondary products will be dependent on the relative compound water solubilities

47 resulting in either Se mobilization towards aquifers or accumulation onto developing soils  
48 and plants. Such studies could prove useful for developing risk assessments in  
49 volcanically active regions on our planet, and for reaching a better understanding of the  
50 global continent-ocean Se isotope budget and signature.

51  
52 **Key words:** low-temperature volcanic emissions, fumaroles; selenium, Se isotopes; Piton  
53 de la Fournaise; Réunion island

## 1. Introduction

Selenium (Se, atomic number 34) is a chalcophile, semi-volatile and redox-sensitive non-metal that naturally occurs in four valence states: -2, 0, +4 and +6 (Johnson and Bullen, 2004) in low- and high-temperature environments on our planet. Over the past decade, significant progress has been made to understand the behavior of Se in terrestrial magmatic systems, especially in conjunction with its chalcophile siblings S and Te (e.g., Jenner et al., 2010; Lissner et al., 2014; Edmonds and Mather, 2017; Yierpan et al., 2018; 2019; 2020). Selenium concentrations in submarine lavas of various geotectonic settings (arc lavas, hot-spot influenced magmatism and MORB glasses) suggest a lack of Se degassing during magmatic differentiation (e.g., Jenner et al., 2010; Jenner et al., 2015; Lissner et al., 2014; Kurzawa et al., 2019; Yierpan et al., 2021). The observed volatility of S compared to the negligible volatility of Se at submarine depths enable Se concentrations and Se/S ratios to be used as estimates for the pre-eruptive S concentrations of mantle melts (e.g., Jenner et al., 2010; 2015; Reekie et al., 2019). Near surface volcanic activities, on the other hand, are associated with significant Se enrichment in eruption plumes and volcanic ashes with respect to the residual volcanic rocks, which points to pronounced subaerial Se degassing (e.g., Davidson and Powers, 1959; Crowe et al., 1987; Allard et al., 2000; Toutain et al., 2003; Floor and Román-Ross, 2012). Global volcanic Se emissions are estimated to be in the range of 100 - 1800 tons per year (e.g., Mosher and Duce, 1987; Nriagu, 1989; Mather et al., 2004), which translates to 50 - 65 % of the total atmospheric Se concentration. On average, volcanic Se gas concentrations range between 0.6 and 3  $\mu\text{g}\cdot\text{g}^{-1}$  in arc settings and between 5 and 40  $\mu\text{g}\cdot\text{g}^{-1}$  in ocean island settings (e.g., Zelenski et al., 2021). Although the anthropogenic Se emissions are sometimes calculated to dominate the atmospheric Se budget during more passive volcanic periods (Wen and Carignan, 2007), exceptions exist at regional scale, such as the island Sicily with its active stratovolcano Etna. Here, volcanic Se emissions surpass those from anthropogenic activities and the biosphere, and constitute the main point source of Se in the entire Mediterranean region (Calabrese et al., 2011). Overall, large variations in Se emission budget observed not only between contrasting volcanic settings such as subduction zones vs. OIBs (Edmonds et al., 2018), but also within one group impede accurate assessments on global volcanic Se gas emissions.

Advancements in mass-spectrometry with respect to Se isotope measurements over the past 10 years allow now the characterization of samples in the  $\text{ng}\cdot\text{g}^{-1}$  concentration range (e.g., Kurzawa et al., 2017; Labidi et al., 2018; Varas-Reus et al., 2019; Yierpan et al., 2020). In the context of our study, Yierpan et al. (2021) showed that volcanic glasses formed at the Reykjanes ridge below ~250 m water depth maintain a magmatic Se budget and isotope signature, while degassed basalts derived from shallower levels exhibit heavier isotope compositions accompanied with lower concentrations. This points to preferential loss of light Se isotopes in the gas phase. Supported by a Rayleigh distillation model, the isotope systematics in the study of Yierpan et al. (2021) strengthen the previous findings of magmatic Se volatilization in reduced form as SeS,  $\text{H}_2\text{Se}$ , and Se(0) (Zelenski et al., 2021) preferentially mobilizing lighter isotopes. However, further mechanisms of Se degassing from volcanic activities are scarce and relatively difficult to quantify. Poorly addressed in the surficial mass-balance are for example, the *i*) Se release from passive lava-lake degassing, *ii*) emanations during cooling of lava flows, and *iii*) fumarole activity in between main eruption events.

In general, volcanic degassing activities are known to release significant amounts of chalcophile elements (S, Cu), heavy metals (Tl, Pb, Hg) and metalloids in quantities that can reach potentially toxic levels to humans (e.g., Rodríguez-Mercado and Altamirano-Lozano, 2013). While the role of Se as a vital micronutrient, reproductive-, metabolic- and antiseptic functions are widely accepted (e.g., Khatiwada and Subedi, 2021; Sunde, 2012), it is also well known that a narrow margin of 40 - 400  $\mu\text{g}$  intake per person per day can cause either Se deficiency or severe toxicity (Rayman, 2000). Therefore, robust constraints on the magnitude of the various near-surface Se emissions are required not only for the assessment of a more precise global inventory, but also for the health safety of the approximately 10 % of the world population living in volcanically active areas (Small and Naumann, 2001) and who are subjected to direct and continuous exposure.

To contribute to a better understanding of the systematics and magnitudes of volcanic Se release from cooling lava flows to the immediate environment, we investigate the Se mass fractions and Se isotope compositions of a unique suite of undegassed and degassed basaltic rocks, as well as various fumarolic products at one of the most active volcanoes in the world, Piton de la Fournaise (PdF) (Peltier et al., 2009; Roult et al., 2012),

Réunion Island (Fig. 1). The fumarolic precipitates are attributed to the 1977, 2007 and 2009 volcanic eruptions and were formed over large temperature gradients (~800 to ~100°C) on the respective lava flows, allowing a consideration of the temperature control in the formation of these products. In detail, the following questions motivated our study:

- 1) What is the Se budget of fumarolic products relative to the degassed melts?
- 2) What are the physicochemical mechanisms and efficiency of Se transfer from volcanic gaseous compounds to surface deposits at PdF?
- 3) What are the most commonly formed mineralogical phases and what is their expected environmental impact?

## **2. Geological setting and sample description**

Piton de la Fournaise is a basaltic shield volcano forming the southeastern part of La Réunion island located in the Indian Ocean (Fig. 1). Together with Mauritius, it represents the youngest volcanic activity on the Mascarene basin, attributed to the same mantle hot-spot that generated the Deccan Traps (Duncan et al., 1989; Lénat et al., 2001). The ca. 2632 m a.s.l. high shield volcano (Liuzzo et al., 2015) is considered one of the most active intraplate volcanoes in the world today; its periodic activity being sometimes compared to Kilauea on the Hawai'i Big Island (Di Muro et al., 2014). The magmatism is dominated by basaltic lava flows with very modest gas release in intracrater fumaroles during dormant periods. Previous geochemical investigations of lavas and extruded mantle xenoliths from La Réunion island concluded that the magmatic source has changed relatively little over time (Albarède et al., 1997; Bosch et al., 2008; Pietruszka et al., 2009; Vlastélic et al., 2009). Therefore, PdF makes an excellent example for a focused investigation of Se fumarole degassing and capture following major active phases.

For this study, basaltic rocks and accompanying fumarolic deposits were sampled during several field campaigns between 2007 and 2011 and comprise products from the eruptions of April 1977, April 2007, and November 2009 (Fig. 1b). The April 2007 eruption lasted 29 days and produced  $210 \cdot 10^6 \text{ m}^3$  of lava at an average rate of  $84 \text{ m}^3 \cdot \text{s}^{-1}$ . It represents the most voluminous eruption of the island in at least two centuries (Staudacher et al., 2009). The November 2009 eruption was a very small event that lasted several hours and produced  $0.14 \cdot 10^6 \text{ m}^3$  of magma at an average rate of  $5.4 \text{ m}^3 \cdot \text{s}^{-1}$ . Both eruptions produced magmas with compositions transitional between alkali and tholeiitic

basalts, with variable amounts of olivine phenocrysts in April 2007. Pre-eruptive magma temperatures were estimated based on the MgO thermometer and ranged between 1174-1196 °C in April 2007 and ca. 1155 °C in November 2009 (Gurioli et al., 2018).

Lava samples include poorly phyrific and olivine-rich lavas and a glassy pumice (REU 091204-3). From these, one of the olivine-rich samples (REU 0704-051) was quenched in a water bucket. Short-lived fumarole deposits were collected at the outlet of a 15-m-deep degassing skylight, at an elevation of 100 to 150 m a.s.l., on the thickest part (ca. 68 m) of the April 2007 lava flow. This vent was repeatedly sampled while its temperature decreased from ~400 to ~300 °C. The collected deposits were previously characterized as aphthitalite ((K,Na)<sub>3</sub>Na(SO<sub>4</sub>)<sub>2</sub>), referred here as Na–K sulfates (Fig. 2b), and thenardite (Na<sub>2</sub>SO<sub>4</sub>). Low-temperature deposits sampled at the surface of the same lava flow were identified as Ca–Mg–Al–(Fe) hydroxy-fluorides, among which ralstonite (Na<sub>x</sub>Mg<sub>x</sub>Al<sub>2-x</sub>(F,OH)<sub>6</sub>·H<sub>2</sub>O), MgAlF<sub>5</sub>·1.5H<sub>2</sub>O, or a mixture of both are the most abundant (see Vlastélic et al., 2013). Also, a low-temperature thenardite crust (0808-292) was collected on the 2007 lava flow at ca. 100 °C. However, as this sample occurred as an incrustation it is very likely that it was initially formed at a higher temperature, dissolved into water and recrystallized at ca 100 °C (Table 1). Gypsum (Ca(SO<sub>4</sub>)<sub>2</sub>H<sub>2</sub>O) was sampled from a lava cave formed as well during the April 2007 eruption. These samples were deposited on the wall of a lava tunnel in which temperature decreased from 200 °C in 2010 to 120 °C during sampling in 2011 (Fig. 2a). Servadio (2011) estimated that between 2007 and 2011, the temperature of the April 2007 lava flow decreased from 1150 °C to 780 °C (at a depth of 15 m). Following the 2009 volcanic activity, freshly produced thenardite powder (sample 0912-0411) was sampled in the November 2009 degassing fractures just after the cessation of the eruption (Fig. 2c). This syn-eruptive deposit formed just above a lava flow at an estimated temperature of ca. 800 °C, in agreement with the thenardite stability field (400-900 °C, Stoiber and Rose, 1974). All details are provided in Table 1. Samples investigated here were subjected to careful microscopic investigations, trace element compositions and Pb isotope ratios by Vlastélic et al. (2013) and Re-Os isotope compositions by Gannoun et al. (2015), who provide further details about the samples.

### 3. Analytical techniques



All measurements were performed following original methods previously established at the Isotope Geochemistry Laboratory, University of Tübingen (Kurzawa et al., 2017; Yierpan et al., 2018). In brief, sample powders equivalent to ~30 ng Se and ~3 ng Te were weighed into conventional Teflon beakers, adding similar amounts of  $^{74}\text{Se}$ - $^{77}\text{Se}$  double-spike and  $^{125}\text{Te}$  single spike, respectively. The sample-spike mixtures were digested with a 5:1 (v/v) mixture of concentrated HF to concentrated  $\text{HNO}_3$  in closed beakers on a hot-plate at 85 °C for 48 hours. Selenium and Te were purified from sample solutions by two-step ion-exchange chromatography. First, we employed an anion exchange column to remove Fe and collect purified Te. Secondly, Se was purified using a cation exchange column to remove the remaining cations.

Tellurium concentrations were determined by hydride generator quadrupole ICP-MS on the iCAP-Qc instrument, and Se isotope abundances and elemental concentrations were measured by hydride generation multi-collector ICP-MS on the ThermoFisher Scientific NeptunePlus instrument of the Isotope Geochemistry Laboratory, University of Tübingen. Typically, currents of 0.8 - 0.9 V were obtained on mass  $^{82}\text{Se}$  during measurements (using an amplifier resistor of  $10^{11} \Omega$ ) for a  $30 \text{ ng} \cdot \text{mL}^{-1}$  Se solution, with operating parameters similar to those reported by Kurzawa et al. (2017). A signal of 32,000 cps on mass  $^{126}\text{Te}$  was obtained for a Te standard solution of  $0.5 \text{ ng} \cdot \text{mL}^{-1}$ , similar to operating parameters reported by Yierpan et al. (2018). Selenium and Te concentrations were determined at similar signal intensities compared to those of standard solutions.

Selenium isotope values are expressed as  $\delta^{82/76}\text{Se}$  in ‰ deviations from the NIST3149 reference material throughout this study. Measurements of the inter-laboratory standard solution MH-495 relative to NIST3149 yielded an average  $\delta^{82/76}\text{Se}$  value of  $-3.25 \pm 0.07 \text{ ‰}$  (2s.d.,  $n=25$ ,  $30 \text{ ng} \cdot \text{mL}^{-1}$  solutions), indistinguishable from results of previous studies (Kurzawa et al., 2017; Labidi et al., 2018; König et al., 2019; König et al., 2021; Varas-Reus et al., 2019; Yierpan et al., 2019; 2020). External reproducibility on  $\delta^{82/76}\text{Se}$  is conservatively expressed as  $\pm 0.12 \text{ ‰}$  (2s.d.), based on replicate digests and measurements of different samples, among which the highly heterogeneous sample 0808293 is the least reproducible ( $0.12 \text{ ‰}$ ,  $n=3$ , 2s.d.). All samples were chemically processed and measured together with international USGS rock reference materials (Table 1). For 3 times digested basalt BCR-2 we obtained on average  $78.6 \text{ ng} \cdot \text{g}^{-1}$  Se,  $2.62$

ng·g<sup>-1</sup> Te, and  $\delta^{82/76}\text{Se}_{\text{NIST3149}} = 0.12 \pm 0.08 \text{ ‰}$  (2s.d.). These results are indistinguishable from values obtained previously (76  $\pm$  3 ng·g<sup>-1</sup> Se, 2.54  $\pm$  0.08 ng·g<sup>-1</sup> Te and  $\delta^{82/76}\text{Se}_{\text{NIST3149}} = 0.23 \pm 0.13 \text{ ‰}$ ,  $n=10$ , compilation by Yierpan et al. [2020]). For one digested diabase W2a, we obtained 103 ng·g<sup>-1</sup> Se, 1.78 ng·g<sup>-1</sup> Te, and  $\delta^{82/76}\text{Se}_{\text{NIST3149}} = -0.09 \pm 0.07 \text{ ‰}$  (2s.e.), indistinguishable from previously obtained 107  $\pm$  3 ng·g<sup>-1</sup> Se, 1.71  $\pm$  0.07 ng·g<sup>-1</sup> Te and  $\delta^{82/76}\text{Se}_{\text{NIST3149}} = -0.07 \pm 0.11 \text{ ‰}$ ,  $n=9$ , (Yierpan et al., 2019). Long-term analytical reproducibility for both Se and Te concentration determination is  $\sim 3 \%$  r.s.d. (1 s.d.;  $n>100$ , Yierpan et al. 2019). All blanks were below detection limit.

#### 4. Results

Along with Se elemental data and isotope ratios for basaltic and fumarolic samples (Table 1), we provide Te concentrations for future reference but keep the following description and discussion focused on Se only. One basaltic glass shows the highest Se content (138 ng·g<sup>-1</sup>) compared to basalts with a crystalline matrix (poorly phyrlic to olivine-rich) that range to lower Se contents (136 to 58 ng·g<sup>-1</sup>). Fumarolic samples are all enriched in Se with concentrations ranging from 0.543 to 1578  $\mu\text{g}\cdot\text{g}^{-1}$ . In detail, Na-K sulfates show decreasing Se contents (1.55 to 0.543  $\mu\text{g}\cdot\text{g}^{-1}$ ) with decreasing condensation temperatures (400 to 325 °C). The low- and high-temperature thenardite samples show respective Se contents of 13.6 and 1.70  $\mu\text{g}\cdot\text{g}^{-1}$ . Gypsum, representing colder deposits (200 to 120 °C), contain between 2.58 to 11.3  $\mu\text{g}\cdot\text{g}^{-1}$  Se, while the Ca–Mg–Al–Fe fluorides and native sulfur with lowest condensation temperatures ( $\sim 100$  °C) incorporate the highest Se mass fraction (82.3 to 370  $\mu\text{g}\cdot\text{g}^{-1}$  and 1578  $\mu\text{g}\cdot\text{g}^{-1}$ , respectively).

Basalt Te concentrations range between 0.12 and 0.3 ng·g<sup>-1</sup>, significantly lower than Atlantic and Pacific MORB values ( $\sim 1.3$  to 6.2 ng·g<sup>-1</sup>, Yierpan et al., 2019, Yierpan et al., 2020), and lower than most fumarolic deposits. The latter have highly variable Te concentrations, with Na-K sulfates displaying the highest Te concentrations by several orders of magnitude (285 - 589 ng·g<sup>-1</sup>). High-T thenardite has a much higher Te concentration (82 ng·g<sup>-1</sup>) than the low-T equivalent (0.26 ng·g<sup>-1</sup>), followed by fluorides with concentrations that range between 7.8 and 0.10 ng·g<sup>-1</sup>, and gypsum samples (1.6 - 0.44 ng·g<sup>-1</sup>). Tellurium concentrations for native sulfur are below the detection limit of the method.

Selenium concentrations in fumarolic deposits are up to four orders of magnitude higher than in basaltic lavas. The relative degree of enrichment compared to other trace elements is quantified by their enrichment factor (EF), defined as per [Eq. 1]:

$$EF_{X/R} = (C_X/C_R)_{\text{gas condensate}} / (C_X/C_R)_{\text{lava}} \quad [\text{Eq. 1}]$$

where  $C_x$  is the concentration of element x and  $C_R$  is the concentration of the refractory element used for normalization. Following the approach of previous studies (Vlastélic et al., 2013; Gannoun et al., 2015), Be is used for normalization because of its low volatility and low abundance in lavas, thereby highlighting the relative enrichment of volatile elements. The lava sample REU 0704-04 (paroxysmal phase of April 2007) which is most enriched in a number of volatile trace metals (Bi, Cd, In, Sn) and thus estimated to be least degassed, is taken as reference for EF calculation (Table 1 and Fig. 2 a, b). Relative to basaltic glass, all fumarolic deposits are enriched in Se in the order Na–K sulfates < thenardite (average) < gypsum (average) < Ca–Mg–Al–Fe fluorides << native sulfur. Apart from the two thenardites (one secondary and one *in situ*), which do not follow a specific pattern, a clear systematic is observed between the formation temperature of fumarolic deposits and their EF Se/Be. The coldest deposits (Ca–Mg–Al–Fe fluorides and especially native sulfur) show the highest Se enrichments, whereas deposits formed well above the sublimation temperature of  $\text{SeO}_2$  [ $\sim 315^\circ\text{C}$ , Devillanova (2007)], are characterized by the lowest Se enrichments (Na–K sulfates).

The  $\delta^{82/76}\text{Se}$  of basaltic glass ( $-0.19 \pm 0.04\text{‰}$  2s.e.) is within uncertainty identical to the average value previously obtained for basaltic glasses from Atlantic and Pacific MORBs ( $\delta^{82/76}\text{Se} = -0.16 \pm 0.12\text{‰}$ , 2s.d.,  $n=31$ , Yierpan et al., 2019). Analyzed basalts with a crystalline matrix show significantly higher  $\delta^{82/76}\text{Se}$  ranging from 0.04 to 0.23 ‰ ( $\pm 0.17\text{‰}$ ,  $n=4$ , 2s.d.). These compositions are within uncertainty identical to previously published data for subaerially erupted basaltic reference materials BHVO-2, BCR-2, BE-N and BIR-1a ( $\delta^{82/76}\text{Se} = 0.15$  to  $0.29 \pm 0.13\text{‰}$  max., 2s.d. Yierpan et al., 2020).

Fumarolic samples extend to both significantly lighter and heavier isotope values ( $\delta^{82/76}\text{Se} = +0.6$  to  $-2.08\text{‰}$ , Fig. 2d) compared to undegassed volcanic glass. Na–K sulfates show decreasing  $\delta^{82/76}\text{Se}$  from  $-0.91$  to  $-1.46\text{‰}$  with decreasing deposition temperatures from 400 to 325 °C. A difference is also seen between the high-temperature

thenardite powder ( $\delta^{82/76}\text{Se} = -0.44 \pm 0.04 \text{ ‰}$ , 2s.e.) and cooler, secondary thenardite ( $\delta^{82/76}\text{Se} = -0.97 \pm 0.05 \text{ ‰}$ , 2s.e.). Gypsum samples extend the trajectory to the most negative  $\delta^{82/76}\text{Se}$  values ( $\delta^{82/76}\text{Se} = -1.37$  to  $-2.08 \text{ ‰}$ ). This is followed by an inversion towards least negative values ( $\delta^{82/76}\text{Se} = -0.55$  to  $-0.94 \text{ ‰}$ , Ca–Mg–Al–Fe fluorides) to even positive ( $\delta^{82/76}\text{Se} = +0.6 \text{ ‰}$ , native sulfur) in coldest deposits.

Altogether, the data show Se-enriched fumarole deposits complementing Se-depleted basalts. With decreasing fumarole depositional temperatures, a tendency towards lighter isotopic compositions is first observed. However, this trend stops with the coldest deposits (fluorides and native sulfur), which display the highest contents and relative Se enrichments and are accompanied by a significant isotope excursion up to positive  $\delta^{82/76}\text{Se}$ .

## 5. Discussion

Mineralogically distinctive fumarolic products were formed at the surface of cooling basaltic lava flows following months after the initial effusive eruption. The fumarolic solid products were formed at the fumarolic gas temperatures measured at the time of sampling. Except for one secondary thenardite, the fumaroles are associated with variable formation temperatures ranging from  $\sim 800^\circ\text{C}$  to  $\sim 100^\circ\text{C}$ . In the following, we address first, the general principles of Se degassing and estimate the emanation factor (degree to which an element is released from the melt) in different tectonic settings and for PdF volcano in more detail, to then suggest mechanisms that can explain the formations of the individual fumarole groups at our study site. Finally, the Se contribution of the fumarolic products to the immediate environment as well as potential implications for human health are addressed.

### 5.1 Constraints on Se volatility and emanation at Piton de la Fournaise

The degree of volatility of a certain element during a volcanic eruption depends on the gas-melt partition coefficients, which are in turn influenced by the element speciation, affinity for ligand formation, sulfur and chlorine content of the system (e.g., Zelenski et al., 2021). Available studies suggest that Se, as a semi-volatile element (condensation temperature,  $T_{50} \sim 428^\circ\text{C}$ , Wood et al., 2019), will be preferentially degassed as hydrides ( $\text{H}_2\text{Se}$ ), free atoms  $\text{Se}(0)$ , as well as  $\text{SeS}$  compounds in equilibrium with  $> \sim 1100^\circ\text{C}$  hot

silicate magma (Tetsuro, 1964; Mason et al., 2021). According to these constraints, higher gas-melt partition coefficients ( $D^{\text{gas-melt}}$ ) are expected in S-rich, reduced hotspot and rift-related volcanism compared to more oxidized arc volcanism. Indeed, calculations made by Zelenski et al. (2021) suggest higher Se  $D^{\text{gas-melt}}$  in hot-spot and rift settings (51 - 329, average of 129) compared to more oxidized arc systems (49 - 56, average of 52). Exceptions are observed, for example, for the subduction-related magmatism of Stromboli (1993-1997) and Ambrym (2007-2008), where Se concentrations in their gas plumes exceeded those of some individual intraplate volcanoes (e.g., Mason et al., 2021). From the studies of Mason et al. (2021) and Zelenski et al. (2021) it can be deduced that the principles and factors influencing Se degassing (and likely the calculation of it) at different geotectonic settings (i.e., hot-spot vs. arc- influenced) require consideration of further parameters such as the total amount of dissolved gas and lava production rate, as well as the less monitored low-temperature degassing from effusive eruptions. Strikingly, the systematics seem more straightforward for elements like Mo, Cu, In, W, Tl, which appear to be consistently more enriched in basaltic gas plumes of arc-related magmatism (Mason et al., 2021) and thus, show a clearer relationship to a specific tectonic setting.

Selenium isotope data corroborate the mechanisms of subaerial Se degassing elaborated above. Here we report a preferential loss of lighter isotopes in the degassed melts ( $\delta^{82/76}\text{Se} = +0.17 \text{ ‰}$ ,  $n = 4$ ) compared to undegassed glass ( $\delta^{82/76}\text{Se} = -0.19 \text{ ‰}$ ,  $n = 1$ ), which agrees with a Se volatilization in reduced form. Similar observations have also been made through experimental studies (Kurzawa et al., 2017) and recent analyses of variously degassed volcanic samples from the Reykjanes ridge (Yierpan et al., 2021).

The emanation coefficient ( $\varepsilon$ ) is defined as the mass fraction of Se degassed. Several strategies have been proposed to calculate  $\varepsilon$  using pre-eruptive and post-eruptive lava compositions, sometimes together with normalizing parameters such as S or Pb (for a comparison see Lambert et al., 1985; Gauthier and Le Cloarec, 1998; Gauthier et al., 2000; Wieser et al., 2020). Here we adapt the equation A1 of Gauthier et al. (2000) to calculate  $\varepsilon$ : Se volatilization of a gas in chemical equilibrium with the magma ( $D^{\text{gas-melt}}$ ), which also includes the theoretically determined, setting-specific fraction of total gas in the undegassed magma [Eq. 2].

$$\varepsilon_{Se} = \frac{\Phi D_{Se}^{gas-melt}}{\Phi D_{Se}^{gas-melt} + 1 - \Phi}$$

[Eq.2]

Where  $\Phi$  is the fraction of gas in the undegassed magma, and a  $\varepsilon_{Se}$  value of 1 would mean complete volatilization of the element. Applying an average  $\Phi$  of 0.008 in volatile-poor hot-spot and rift settings, and a  $\Phi$  of 0.04 for volatile-rich arc settings (i.e., 0.8 % and 4 % respectively, Bureau et al., 1999; Plank et al., 2013), together with the  $D_{Se}^{gas-melt}$  presented above, we obtain a  $\varepsilon_{Se}$  in the range of 0.29 to 0.73 for hot-spot and rift settings and between 0.67 and 0.70 for arc settings. We can now estimate the  $\varepsilon_{Se}$  at PdF using our measured Se concentration data (olivine corrected values in Table 1) and assuming a primary melt (PM) composition of  $0.2 \mu\text{g}\cdot\text{g}^{-1}$  Se (Collins et al., 2012). In this case,  $\varepsilon_{Se}$  is calculated in the range of 0.31 - 0.53 ( $= [\text{Se}_{PM} - \text{Se}_{lava}] / \text{Se}_{PM}$ ), which agrees with the general estimate discussed above. Combining the average lava production rate (ALPR) at PdF volcano ( $16\cdot 10^6 \text{ m}^3\cdot\text{a}^{-1}$ , dense rock equivalent, Roult et al., 2012) and the typical lava density ( $\rho = 2700 \text{ kg}\cdot\text{m}^{-3}$ ) yields that between 2.7 and 4.6 tons of Se potentially volatilize every year at this site ( $= \text{Se}_{PM} \cdot \text{ALPR} \cdot \rho \cdot \varepsilon_{Se}$ ). Deviations from this range are expected during larger volcanic eruptions. As such, by using the dense rock equivalent volume of degassing melt of  $58\cdot 10^6 \text{ m}^3$  ( $V^{2007}$ ) from Di Muro et al. (2014), yields that the high-rate eruption of April 2007 emitted between 10 and 17 tons of gaseous Se ( $= \text{Se}_{PM} \cdot V^{2007} \cdot \rho \cdot \varepsilon_{Se}$ ). These values are between 100 and 1000 times higher than during the 2009 activity, which erupted at a lower rate. We conclude that significant amounts of Se escape from the Earth's interior during volcanic eruptions as component in aerosols ( $> 1000^\circ$ ) and fumarolic products ( $\sim 800 - 100^\circ\text{C}$ ). In this study we assess the mechanism of Se emanation and isotope fractionation during basaltic lava cooling which leads to the formation of fumaroles.

## 5.2 Selenium capture in fumarolic deposits – a mineralogical control?

Fumarole minerals form by condensation through the interaction of hot gases with the cold atmosphere or by gas-rock interactions (e.g., Stoiber and Rose, 1974; Getahun et al., 1996). Initially degassed Se species are most likely to be reduced, however rapid

convergence with the cold atmosphere is expected to trigger a series of oxidative reactions. During these processes, hydrogen selenide ( $\text{H}_2\text{Se}$ ) can be oxidized to elemental Se ( $\text{Se}^0$ ),  $\text{SeO}_2$ , and further to  $\text{SeO}_3$ , accompanied by saturation of the compounds favoring precipitation (Wen and Carignan, 2007). Therefore, Se concentration and isotopic composition in fumarolic deposits can reflect the ability of gaseous Se species to enter the various crystal networks of the minerals. Possible mineral-specific reactions include  $\text{Se}^0$  substitution for  $\text{S}^0$  in native sulfur as the ionic radii and electronegativities of the two elements are very similar. The same applies for  $\text{Se}^{-2}$  substitution for  $\text{S}^{-2}$  (Shannon, 1976). However, in other oxidation states these parameters change substantially, and  $\text{Se}^{4+}$  substitution for  $\text{S}^{4+}$  is unlikely. Condensation of other compounds like  $\text{SeF}_4$  (102°C boiling point) might also occur, and although Se partitioning into S-free fluoride minerals is rather poorly constrained, it must involve chemical reactions either in the gas phase (as  $\text{SeF}_4$  is a volatile compound) or at the surface of the precipitated mineral. In a recent comprehensive study of fumarole deposits from Fogo volcano, Cape Verde, Silva et al. (2019) suggested that  $\text{SeF}_{4(g)}$  condensation can be facilitated due to  $\text{Se}^{4+}$  sequestration into oxygen pyramids.

It is thus plausible that the chemical processes (such as oxidation) involving Se incorporation into thenardite, sulfates and potentially gypsum can be different than those governing Se capture into fluoride and elemental sulfur minerals. In the following model, we assume that: *i*) each mineral is in equilibrium with a gas with a constant isotopic composition but at different temperatures reflecting the formation temperature of that mineral. Isotopic effects imparted on the gas by a given mineral are assumed to not influence other minerals, which formed from independent gas aliquots; *ii*) all mineral phases represent individual mineral end-members in equilibrium with the gas, meaning that individual fractionation factors ( $\alpha$ ) will be at play. As a starting point, we assume that *i*) the initial  $\delta^{82/76}\text{Se}$  of the gas is relatively close to the composition of the hottest sample (~800 °C thenardite, -0.44 ‰), and that *ii*) condensation of Se is very small, with no effect on the Se isotope composition of the gas. The observed isotopic variation in fumaroles is thus governed primarily by the Se oxidation state in the respective minerals: +6 in sulfates (including thenardite and gypsum), +4 in fluorides, and 0 in native sulfur.

Fig. 3 shows expected or calculated individual linear relationships between the isotopic composition of the mineral and that of the gas ( $\Delta^{82/76}\text{Se}$ ), in accordance with the

general theory of isotopic fractionation between two phases. Namely,  $\Delta^{82/76}\text{Se}$  (Phase A – Phase B) varies linearly with  $1/T$  at low temperature and  $1/T^2$  at high temperature [Eq. 3]:

$$\Delta^{82/76}\text{Se}_{\text{mineral-gas}} = \delta^{82/76}\text{Se}_{\text{mineral}} - \delta^{82/76}\text{Se}_{\text{gas}} = 1000\ln\alpha_{\text{mineral-gas}} = A+B / T^2 \quad [\text{Eq. 3}]$$

Alternatively, one could address the “mineral-gas” relationship as “oxidized-reduced” fractions. The  $\Delta^{82/76}\text{Se}_{\text{mineral-gas}}$  variations observed for the mineral group consisting of the most oxidized Se compounds,  $\text{Se}^{\text{VI}}$  (thenardite, sulfates and gypsum) most likely reflect the increase of mineral-gas isotope fractionation with decreasing  $T$ . Additionally, but not necessarily, a kinetic effect could also be at play during the formation of the hotter phases. This hypothesis is suggested based on the observed linear relationship between  $\delta^{82/76}\text{Se}$  and temperature. The combination between significantly higher Se concentrations and Se present as  $\text{Se}^{\text{IV}}$  in fluorides can in turn be explained through a rapid condensation from gaseous  $\text{SeO}_2$ . The smaller  $\Delta^{82/76}\text{Se}_{\text{mineral-gas}}$  of fluorides compared to the more oxidized end-members sulfates and gypsum also points at the dominance of  $\text{SeO}_2$  and likely  $\text{Se}^0$  species in the gas phase (Fig. 3). The latter is required to explain the extremely high Se concentrations (up to 1.6 wt. %) in native sulfur, where a  $\text{Se}^0 - \text{S}^0$  substitution, and thus the simplest and most direct reaction likely facilitates the enrichment. In support of this, the presence of  $\text{Se}^0$  in volcanic gas has been previously observed (Bichler et al., 1995).

Altogether, the preferential incorporation of variably oxidized Se species into the crystal lattice of individual fumarolic minerals could have resulted in the observed isotope variations. At this stage, we have to emphasize that little work has been done on oxidation reactions, and mostly in aqueous solutions (e.g., Johnson and Beard, 1999; Johnson, 2004; Wasserman et al., 2021), and none at all exist for gas-phase reactions. The situation becomes even more uncertain if a potential kinetic effect is coupled to one or several oxidation reaction(s). Although simple kinetic effects tend to produce light products, some of the individual oxidation steps within the overall reaction could, if they are able to attain equilibrium, result in isotopically heavy products. We conclude that *i*) the observed light Se isotopic composition of the sulfate minerals could reflect a kinetic isotope effect related to oxidation, and that *ii*) experimental studies could contribute to a clearer understanding of the isotope signatures of variably oxidized fumarolic precipitates.



### 5.3 Temperature-dependent Rayleigh condensation

The formation of individual fumarole minerals at certain temperatures as the lava and gases cool down invites us to test the hypothesis of a temperature-dependent condensation process and potential Se isotope fractionation due to this effect. This model assumes that instead of the oxidation state, the relative near-surface stability of Se compounds (as a function of temperature) plays a decisive role in the Se partitioning into the fumarolic mineral phases. The condensation hypothesis can be independently evaluated with Se stable isotopes. Although condensation can involve several reactions between multiphase gas and solid reservoirs, we consider a single isotopic exchange reaction accounting for the bulk condensation process. The corresponding coefficient of isotopic fractionation for this reaction, is defined as Eq. 4.

$$\alpha_{s/g} = (^{82/76}\text{Se})_{(s)} / (^{82/76}\text{Se})_{(g)} \quad [\text{Eq. 4}]$$

for both equilibrium and kinetic isotope fractionation where (s) and (g) are for the bulk solid and bulk gas, respectively. Here, the temperature dependence of Se isotopes suggest that equilibrium fractionation is the dominant process. This does not exclude the fact that kinetic fractionation can be temperature dependent too, however gaseous diffusion or evaporative effects tend to show a lack of temperature dependence (e.g., Schauble 2004). In a similar manner as for the mineral-dependent model presented above, we assume that all deposits derive from fractional condensation of the same high-temperature parental gas, with an isotope composition close to the hottest thenardite ( $\delta^{82/76}\text{Se} = -0.44 \text{ ‰}$ ). The general differential equation for a Rayleigh process writes (Criss et al., 1999; Eq. 5):

$$d\ln(^{82/76}\text{Se})_g = (\alpha_{s/g} - 1) d\ln f \quad [\text{Eq. 5}]$$

where  $(^{82/76}\text{Se})_g$  is the isotope ratio of the gas and  $f$  is the mass fraction of Se remaining in the gas phase. When  $\alpha_{s/g}$  is constant, the well-known solution of [Eq. 5] is:

$$(^{82/76}\text{Se})_g = (^{82/76}\text{Se})_i \cdot f^{(\alpha_{s/g} - 1)} \quad [\text{Eq. 6}]$$

where  $(^{82/76}\text{Se})_i$  is the initial ratio of the gas. According to Eq. 6, both gas and condensate  $^{82}\text{Se}/^{76}\text{Se}$  ratios will evolve in the same direction during the condensation process, continuously increasing if  $\alpha_{s/g} < 1$  and continuously decreasing if  $\alpha_{s/g} > 1$ . Consequently, no constant  $\alpha_{s/g}$  matches the  $^{82/76}\text{Se}$  evolution of the deposits. Conversely, increasing the magnitude of isotopic fractionation between the solid and gas phases as condensation proceeds can reproduce the initial decrease and subsequent increase of  $^{82/76}\text{Se}$ . This is shown on the basis of two numerical integrations of Eq. 5 assuming a linear and a non-linear relationship between  $f$  and  $\alpha$  as a function of  $T$  (Fig. 4 a and b). For this, we used an iterative method where the value of  $f$  is changed incrementally. This means that for each value of  $f$  we calculate the relevant value of  $\alpha$  (using the chosen  $\alpha$  vs.  $f$  equation given in figure caption), the incremental change  $d\ln(f)$  and, using the differential Eq. 5, the incremental change  $d\ln(^{82}\text{Se}/^{76}\text{Se})$ . At each step,  $d\ln(^{82}\text{Se}/^{76}\text{Se})$  is added to the preceding value of  $\ln(^{82}\text{Se}/^{76}\text{Se})$ . The calculation is repeated successively from  $f=1$  to  $f=0$  to produce the curves shown in Fig. 4. In both scenarios, the initial gas fractionates solid deposits enriched in the lighter Se isotope ( $\alpha_{s/g} < 1$ ). The size of isotopic fractionation is very small at high temperature but increases as temperature decreases, so that the gas accordingly evolves toward higher  $^{82/76}\text{Se}$ , only subtly at first, but more rapidly as condensation proceeds. At the point where the gas  $^{82/76}\text{Se}$  rises faster than the difference between the two phases ( $\Delta^{82/76}\text{Se} = 1000\ln\alpha_{s/g}$ ), the evolution of the condensates trends reverse (Fig. 4 a and b). In the absence of constraints on how  $\alpha_{s/g}$  varies with  $f$ , the linear model (Fig. 4a) predicts that decreasing  $\alpha_{s/g}$  linearly from 0.9995 at  $f=1$  to 0.9940 at  $f=0$  ( $\alpha_{s/g} = 0.0055 \cdot f + 0.9940$ ) matches the measured data, and yields the lightest  $^{82/76}\text{Se}$  ratios of gypsum at ca. 50 % Se condensation. The second model in Fig. 4b shows that a non-linear decrease of  $\alpha$  from 0.9995 at  $f=1$  to 0.9970 at  $f=0$ , following the relationship  $\alpha_{s/g} = 0.0025 \cdot f^5 + 0.9970$  offers the best fit for the data, yielding the  $\delta^{82/76}\text{Se}$  minimum for the gypsum (-2 ‰) at ca. 30% Se condensation. The low Se concentrations in the minerals deposited between 800 and  $\sim 300^\circ\text{C}$  suggest little change in  $f$  over this temperature segment, whereas at lower  $T$ , small changes in  $T$  trigger rapid loss of Se and therefore a greater change in  $f$  and  $\alpha$  as a function of  $T$ . We therefore suggest that the non-linear model (Fig. 4b) likely represents a better reflection of the reality. Both models explain the trajectory towards positive  $\delta^{82/76}\text{Se}$  values in the late-stage deposits ( $< 315^\circ\text{C}$ ) where isotopic fractionation between gas and solid increases with decreasing temperature. In detail, this temperature dependency is

also observed at a smaller scale within the Na-K sulfate samples suite, which shows decreasing  $\delta^{82/76}\text{Se}$  (from -0.91 to -1.46 ‰) and increasing Se content (from 0.54 to 1.5  $\mu\text{g}\cdot\text{g}^{-1}$ ) as temperatures drop from > 400 to 325°C.

The sublimation temperature of  $\text{SeO}_2$  below ~315°C (Tetsuro, 1964) likely plays a critical role in explaining the highest Se concentrations and thus near-quantitative precipitation in the coldest products (fluorides and elementary sulfur, Fig. 4). In addition, the return to less fractionated Se isotopes and even towards positive  $\delta^{82/76}\text{Se}$  may also be used in favor of a condensation reaction. Further support for this model comes from the results of an earlier experiment deploying a silica tube emplaced in a crack on the roof of a lava tunnel of Piton de la Fournaise (see Toutain et al., 1990). This experiment allowed the investigation of Se condensation merely as a function of temperature as the amount of oxygen is expected to remain relatively constant along the tube. The data of Toutain et al. (1990) are plotted together with our fumarole compositions in Fig. 2c and show an almost logarithmic increase in Se concentration with a gradual decrease in temperature, namely the highest Se condensation in the coldest products below ~315°C. Importantly, the chemical compositions of the silica-tube sublimates differ from the natural fumarolic products investigated in this study, potentially hinting at a rather minor importance of the resulting mineral phases *per se*. Nevertheless, the SEM images of the sublimates in the Toutain et al. (1990) study revealed the occurrence of  $\text{SeO}_2$ -rich minerals such as chalcocite ( $\text{Cu}_2\text{Se}$ ) at the cold end of the silica tube, which was not found as individual cold (< 315°C) fumarolic deposits in this study.

#### 5.4 A brief comparison between the two suggested models

One important criterion of the mineralogical control model, which is based on the oxidation state of the individual Se compounds, is the assumption that the Se isotope composition of the gas does not change during cooling. Thus, the amount of Se trapped in fumarole deposits would need to be extremely small. While these conditions may be met for the sulfates, thenardite and gypsum as their low Se content suggests little depletion and fractionation of the gas, the opposite is observed for the colder, significantly more Se enriched deposits. Also, until further experimental observations and investigations of natural fumarolic products at other sites are available, the contrasting picture of lighter isotope composition in the more oxidized mineral species and heavier in the more reduced

compounds remains unexplained. The proposed Rayleigh condensation models, on the other hand, provide a very plausible explanation for the Se isotope signatures of degassing lava and complementary fumarole deposits as a function of decreasing temperature ( $\leq 800 - 100$  °C). By analogy, a similar condensation model explains the Zn isotope data at Merapi volcano (Toutain et al., 2008). It also clarifies the most dramatic Se concentrations of the deposits formed  $< 315$  °C in agreement with experimental determination of  $\text{SeO}_2$  sublimation temperature. According to this model, up to 80 % of Se emanated by the cooling lava will be re-captured onto the Earth's surface by condensation (Fig. 4). While this model does not rule out mineral-dependent reactions, it also shows that they are not necessarily required to explain the data. In fact, contrary to the mineral model, the temperature-dependent model does not leave any unexplained observations. Based on our investigation, we infer that the effect of non-linear temperature-dependent condensation is likely the primary cause of the observed Se fumarolic signature. However, at this point we do not rule out a modest mineralogical control that does not disturb the observed temperature trend.

## **5.5 Environmental relevance of volcanic fumarole precipitates**

The environmental significance of the fumaroles is determined by the mobility, i.e., solubility and bioavailability or accumulation of the Se-bearing compounds. Further geochemical processes, i.e., complexation and oxidation, change in pH conditions, are also expected to influence the Se behavior in developing soils and surrounding aquifers. Results of experimental studies conducted under controlled conditions have shown that selenite ( $\text{SeO}_3^{2-}$ ) is more stable in neutral to slightly acidic soils and under less oxic conditions (e.g., temperate climate), while selenate ( $\text{SeO}_4^{2-}$ ) will be favored by oxic and alkaline conditions (e.g., tropical climate; Balistrieri and Chao, 1990; Fordyce, 2005; Wijnja and Schulthess, 2000; Wu et al., 2000; Peak and Sparks, 2002). Selenate is extremely susceptible to leaching and is considered bioavailable to plants and food crops to a greater extent than selenite (Bitterli et al., 2010). At the same time,  $\text{SeO}_3^{2-}$  capture and retention has been observed to occur onto developing soils, especially in the presence of poorly crystalline Al-Fe phases (e.g., John et al., 1976; Nakamaru et al., 2005, 2006; Nakamaru and Sekine, 2008). Lastly, metal selenides (e.g.,  $\text{ZnSe}_2$ ,  $\text{FeSe}_2$ ,  $\text{NiSe}_2$ ) and elemental Se potentially released to the topsoil from the reduction of selenite in the

561 presence of dissolved organic carbon (Bruggeman et al., 2007) are extremely immobile  
562 and bio-unavailable and can lead to accumulation. In this context, the fumarolic deposits  
563 are expected to have variable primary solubilities, with sulfates, thenardites and gypsum  
564 generally carrying a smaller amount of Se being the most soluble and gypsum being  
565 moderately water-soluble. Fluorides and native sulfur that are extremely enriched in Se  
566 (0.1 to 1.6 wt. %), being the least soluble phases, are expected to accumulate their Se in  
567 soils, potentially leading to higher concentrations in plants and crops.

568         In the months to years following an eruption, the persisting high temperature in the  
569 core of a lava flow will impede the penetration of rainwater through near-surface boiling  
570 and evaporation. However, as soon as the temperature approaches  $< 100\text{ }^{\circ}\text{C}$ , rainwater  
571 infiltration can leach or even completely dissolve fumarolic deposits in a matter of weeks.  
572 Such a scenario has been observed following the venting of a lava cave formed during  
573 the April 2007 eruption, where the penetration of runoff rainwater dissolved nearly all  
574 gypsum fumarolic deposits (Fig. 5). During such an event, the chemical parameters of the  
575 rainwater (e.g., pH properties) can significantly influence the Se speciation (Fig. 6),  
576 leading to some dramatic re-mobilization events, in extreme scenarios such as those  
577 observed along the flanks of Mt. Etna (Calabrese et al., 2011). Furthermore, sudden  
578 dramatic enrichments can result in unexpected Se concentration increase in the  
579 surrounding aquifers, which can surpass the WHO recommended concentration of  $10\text{ mg}\cdot\text{L}^{-1}$   
580 (John et al., 1976).

581         We encountered several unknowns while attempting to establish a relative mass  
582 balance of environmental Se contribution from the individual fumarolic products. One  
583 major requirement will be to assess the distribution and abundance of the mineral phases,  
584 which can only be achieved through comprehensive mapping. Such an investigation will  
585 rely on a hyperspectral image of the lava flow with individual calibration for the different  
586 minerals. To our knowledge, no such method has yet been designed or published. A  
587 solution will be to tackle the environmental impact through combined investigations of Se  
588 concentrations and isotopic compositions in soils and riverine Se. Furthermore,  
589 distribution comparisons should be made between populated and agricultural areas, as  
590 well as pristine locations to ensure the health safety of the humans living on and with the  
591 volcanic landscape.

## Conclusions

The long-term activity of the Piton de la Fournaise shield volcano emanates, on average, between 2.7 and 4.5 tons of gaseous Se per year. Selenium concentrations and isotope compositions of undegassed and degassed lavas support the preferential Se release in reduced form, inducing the enrichment of light isotopes in the gas phase. Secondary fumarolic minerals (consisting of thenardites, sulfates, gypsum, fluorides and native sulfur at this site) were formed by condensation from gas at the surface of cooling lava flows at temperatures between  $\sim 800^{\circ}\text{C}$  and  $\sim 100^{\circ}\text{C}$ . Combined Se concentration- and isotope analyses of individual fumarolic phases allowed us new insights into the mechanisms of near-surface Se capture. Altogether, the following conclusions are drawn from this study:

- (1) All fumarolic products display significantly higher Se concentrations than degassed and undegassed lavas pointing at the environmental relevance of this Se source in volcanic areas.
- (2) Apart from native sulfur, all minerals carry a light Se isotope signature in accordance with the composition of the gas, and complementing the heavier isotope composition of the degassed lavas.
- (3) In minerals where Se is likely to be present as oxidized species (thenardite, sulfate, gypsum) and which were formed at temperatures  $\sim 800$  to  $> 315^{\circ}\text{C}$ , the most negative  $\delta^{82/76}\text{Se}$  (as low as  $-2.08 \pm 0.06 \text{ ‰}$ ) and lower Se concentrations of max.  $13 \mu\text{g}\cdot\text{g}^{-1}$  are detected.
- (4) Mineral species identified to incorporate less oxidized Se compounds (fluorides and native sulfur) and which are likely precipitated below the sublimation temperature of  $\text{SeO}_2$  show less negative (fluorides,  $\delta^{82/76}\text{Se} = -0.94$  to  $-0.55 \text{ ‰}$ ) to positive  $\delta^{82/76}\text{Se}$  (native sulfur;  $\delta^{82/76}\text{Se} = 0.6 \text{ ‰}$  on average) and very high Se concentrations (0.1 to 1.6 wt. %).
- (5) Se concentrations and isotopic compositions of the fumaroles can be entirely reconstructed through Rayleigh condensation mechanisms as a function of decreasing gas temperature, i.e., increasing gaseous compound instability. Based on isotope data, this model estimates that as much as 80 % of the melt emanated Se is potentially captured by fumarolic phases. According to this model, no other processes are needed to explain the observed patterns.

- (6) A phase-dependent fractionation between more oxidized and reduced Se compounds, could tentatively explain an isotope variation, and particularly the highest Se concentration in native sulfur, which is most likely to have occurred through the exchange between gaseous Se<sub>0</sub> and Se<sub>0</sub> within the S<sub>0</sub> solid phase. Further investigations are needed to shed more light on the isotope fractionation mechanisms in products formed by a potential effect of kinetically induced oxidation in gas-solid systems.
- (7) Based on the available data, we conclude that a combination of modest mineralogical and mostly T-dependent kinetical effects leads to the Se capture in fumaroles.
- (8) The environmental impact of fumarolic Se will be dependent on the oxidation state of the compounds, with oxidized species being generally more mobile in aqueous media than reduced ones. In this context, it is expected that most of the Se originating from native sulfur and perhaps fluoride fumarolic deposits will accumulate onto soils and eventually plants, while leaching of sulfates will mobilize Se towards aquifers. Monitoring the two pools is necessary to understand the relative fluctuation levels and potential consequences for humans and animals due to high levels of Se.
- (9) Fumarolic deposits might constitute an important end-member in the oceanic Se mass-balance and ocean water Se isotope composition and requires careful consideration in these calculations. Complementary studies of Se concentrations and isotope ratios in fumarolic products at other volcanically active sites will help expand our knowledge on the mechanisms of Se recycling from the Earth's interior back to its surface.

## Acknowledgments

C.R., S.K., and M.I.V.R., acknowledge the ERC Starting Grant project O<sub>2</sub>RIGIN (636808) to S.K. for funding this research. M.I.V.R. additionally acknowledges funding from the DFG project VA 1568/1-1. C.R. acknowledges funding from the Excellence Strategy of the State of BW and University of Tübingen for young postdocs (PRO-ROSCA-2021-11). A. Finizola, T. Staudacher and J-P. Toutain are thanked for their participation in the fumarole sampling. Eva Stüeken and one anonymous reviewer are thanked for their constructive

comments and suggestions. Ronny Schoenberg is thanked for his continuous support as head of the Tübingen isotope geochemistry group. Elmar Reitter and Ilka Kleinhanns are thanked for maintaining the clean laboratory at the highest standards.

## Figure captions

**Fig. 1 a)** Schematic map of the Réunion island located in the SW Indian Ocean (top right corner), highlighting the location of Piton de la Fournaise caldera; **b)** Map of Piton de la Fournaise volcano showing the location of the 2007 and 2009 lava flows and the samples of this study, as well as the native sulfur sample from the eruption of 1977 collected from deposits on the eastern side of the flank.

**Fig. 2** Relationships between **a)** EF Se/Be vs. formation temperature; **b)** EF Se/Be vs. Se  $\text{ng}\cdot\text{g}^{-1}$ ; **c)** Se  $\mu\text{g}\cdot\text{g}^{-1}$  vs. formation temperature of the fumarolic deposits of this study together with silica-tube condensates data of Toutain et al. (1990); **d)** Se isotope composition vs. formation temperature. Light grey shaded areas represent the temperature range below the sublimation temperature of  $\text{SeO}_2$  ( $< 315^\circ\text{C}$ ). For simplicity, the average value obtained from two individual digests of the native sulfur is plotted. Legend to all plots is shown in panel b). Bulk Silicate Earth (BSE)  $\delta^{82/76}\text{Se}$  in panel d) is from Varas-Reus et al. (2019). Uncertainty bars are smaller than the symbols.

**Fig. 3** Plot of  $\Delta^{82/76}\text{Se}_{(\text{mineral-gas})}$  versus temperature ( $10^6/T^2$  in K) where  $\Delta^{82/76}\text{Se}_{(\text{mineral-gas})} = \delta^{82/76}\text{Se}_{\text{mineral}} - \delta^{82/76}\text{Se}_{\text{gas}}$ .  $\delta^{82/76}\text{Se}_{\text{gas}}$  is assumed to be constant and identical to the value of the hottest thenardite ( $-0.44\text{‰}$ ) (dashed line). This representation assumes that all minerals equilibrate at different temperatures with a gas of constant Se isotope composition. The formation of sulfates (thenardite, K-Na sulfates and gypsum) over a wide temperature range allows the T-dependency of  $\Delta^{82/76}\text{Se}$  ( $\text{Se}^{\text{VI}}$ - gas) to be quantified (linear regression). The temperature control on  $\Delta^{82/76}\text{Se}$  ( $\text{Se}^{\text{IV}}$ - gas) and  $\Delta^{82/76}\text{Se}$  ( $\text{Se}^0$ - gas) cannot be evaluated because fluoride ( $\text{Se}^{\text{IV}}$ ) and native sulfur ( $\text{S}^0$ ) form only at low temperatures. Interrupted light grey lines between gas and fluorides as well as gas and native sulfur represent expected trends. This plot suggests a possible relationship between  $\Delta^{82/76}\text{Se}_{(\text{mineral-gas})}$  and selenium oxidation state in minerals.



**Fig. 4.** Evolution of the Se isotope composition of the gas and solid phases calculated using numerical integrations of Eq. 5. In both models, the initial gas is assumed to have the same composition as the 800°C thenardite (-0.44 ‰). Model **a**) is based on a linear relationship between  $f$  and  $\alpha$  as a function of  $T$ . Here,  $\alpha_{s/g}$  varies linearly from 0.9995 at  $f = 1$  to 0.994 at  $f = 0$  ( $\alpha_{s/g} = 0.0055 \cdot f + 0.994$ ). Model **b**) describes a non-linear relationship between  $f$  and  $\alpha$ , where  $\alpha_{s/g}$  varies non-linearly from 0.9995 at  $f = 1$  and 0.9970 at  $f = 0$  ( $\alpha_{s/g} = 0.0025 \cdot f^5 + 0.9970$ ). The gas curve (dashed line) is plotted versus the mass fraction of Se remaining in the gas ( $f$ ). The evolution of the solid phase (solid line) is inferred from  $\alpha_{s/g}$ . Because we cannot accurately estimate the  $\text{Se}/\text{Se}_i$  in the individual fumarolic minerals, we theoretically indicate their distribution in the models according to their  $\delta^{82/76}\text{Se}$  composition.

**Fig. 5 a)** Gypsum (with Cu sulfates) deposits that were sampled from the lava cave AF1105 (eruption April 2007), and **b)** a close-up photo of the remaining of the same gypsum deposits following venting of the lava cave and penetration of runoff water which dissolved and mobilized all gypsum (and by analogy also the incorporated Se). Photos were taken and kindly provided by A. Finizola (University of Reunion).

**Fig. 6** Schematic illustration of the different stages of lava cooling and near-surface fumarole formation in the context of Se degassing. The indicated temperature is that of the gas fraction. Unlike S, a large fraction of Se remains soluble in high-temperature lava flows during the syn-eruptive phase (Stage 1). The largest Se release occurs at lower temperatures (~315 to 100°C; Stage 3). Exsolution of F during the very late stage of crystallization promotes Se volatilization as  $\text{SeF}_4$  or  $\text{SeF}_6$ . Dissolution and leaching of fumaroles through penetrating rainwater mobilize oxidized Se into aquifers. Adsorption onto Al-Fe phases in young soils accumulates Se. The zoom-in depiction of the cooling lava shows the progressive formation of fumarolic deposits on top of lava flows, in caves and within cavities of the solidified lava (microscopic scale). Sulfur deposits are shown in bright yellow, thenardite in grey, gypsum and fluorides are shown in white-bluish colors. Note that deviations from these colors are possible depending on the respective incorporation of trace elements.

## References

- Albarède, F. et al., 1997. The Geochemical Regimes of Piton de la Fournaise Volcano (Réunion) During the Last 530 000 Years. *Journal of Petrology*, 38(2): 171-201.
- Allard, P. et al., 2000. Acid gas and metal emission rates during long-lived basalt degassing at Stromboli Volcano. *Geophysical Research Letters*, 27(8): 1207-1210.
- Balistrieri, L.S., Chao, T.T., 1990. Adsorption of selenium by amorphous iron oxyhydroxide and manganese dioxide. *Geochimica et Cosmochimica Acta*, 54(3): 739-751.
- Bichler, M., Poljanc, K., Sortino, F., 1995. Determination and speciation of minor and trace elements in volcanic exhalations by INAA. *Journal of Radioanalytical and Nuclear Chemistry*, 192: 183 - 194.
- Bitterli, C., Bañuelos, G.S., Schulín, R., 2010. Use of transfer factors to characterize uptake of selenium by plants. *Journal of Geochemical Exploration*, 107(2): 206-216.
- Bosch, D. et al., 2008. Pb, Hf and Nd isotope compositions of the two Réunion volcanoes (Indian Ocean): A tale of two small-scale mantle “blobs”? *Earth and Planetary Science Letters*, 265(3): 748-765.
- Criss, R.E. (1999) in Bottrell, S. (2003) *Principles of Stable Isotope Distribution*. 254 pp. New York, Oxford: Oxford University Press. ISBN 0195117751. *Geological Magazine*, 140(2): 233-233.
- Bruggeman, C., Maes, A., Vancluysen, J., 2007. The interaction of dissolved Boom Clay and Gorleben humic substances with selenium oxyanions (selenite and selenate). *Applied Geochemistry*, 22(7): 1371-1379.
- Bureau, H., Métrich, N., Semet, M., Staudacher, T., 1999. Fluid-magma decoupling in a hot-spot volcano. *Geophysical Research Letters* 23: 3501-3504.
- Calabrese, S. et al., 2011. Atmospheric sources and sinks of volcanogenic elements in a basaltic volcano (Etna, Italy). *Geochimica et Cosmochimica Acta*, 75(23): 7401-7425.
- Collins, S.J., MacLennan, J., Pyle, D.M., Barnes, S.J., Upton, B.G.J., 2012. Two phases of sulphide saturation in Réunion magmas: Evidence from cumulates. *Earth and Planetary Science Letters*, 337-338: 104-113.
- Crowe, B.M., Finnegan, D.L., Zoller, W.H., Boynton, W.V., 1987. Trace element geochemistry of volcanic gases and particles from 1983–1984 eruptive episodes of Kilauea Volcano. *Journal of Geophysical Research: Solid Earth*, 92(B13): 13708-13714.
- Davidson D.F., and Powers H.A., (1959) Selenium content of some volcanic rocks from western United States and Hawaiian Islands. Bulletin 1084-C, USGS Numbered Series. U.S. Govt. Print. Off. doi: 10.3133/b1084C.
- Devillanova, F.A., 2007. *Handbook of Chalcogen Chemistry: New Perspectives in Sulfur, Selenium and Tellurium*. Royal Society of Chemistry.
- Di Muro, A. et al., 2014. The Shallow Plumbing System of Piton de la Fournaise Volcano (La Réunion Island, Indian Ocean) Revealed by the Major 2007 Caldera-Forming Eruption. *Journal of Petrology*, 55(7): 1287-1315.
- Duncan, R.A., Backman, J., Peterson, L., The Shipboard Scientific, P., 1989. Reunion hotspot activity through tertiary time: Initial results from the ocean drilling program, leg 115. *Journal of Volcanology and Geothermal Research*, 36(1): 193-198.

- Edmonds, M., Mather, T.A., 2017. Volcanic Sulfides and Outgassing. *Elements*, 13(2): 105-110.
- Edmonds, M., Mather, T.A., Liu, E.J., 2018. A distinct metal fingerprint in arc volcanic emissions. *Nature Geoscience*, 11(10): 790-794.
- Floor, G.H., Román-Ross, G., 2012. Selenium in volcanic environments: A review. *Applied Geochemistry*, 27(3): 517-531.
- Fordyce, F., 2005. Selenium; in *Essentials of Medical Geology*. Academic Press, 373-415 pp.
- Gannoun, A., Vlastélic, I., Schiano, P., 2015. Escape of unradiogenic osmium during sub-aerial lava degassing: Evidence from fumarolic deposits, Piton de la Fournaise, Réunion Island. *Geochimica et Cosmochimica Acta*, 166: 312-326.
- Gauthier, P.-J., Le Cloarec, M.-F., 1998. Variability of alkali and heavy metal fluxes released by Mt. Etna volcano, Sicily, between 1991 and 1995. *Journal of Volcanology and Geothermal Research*, 81(3): 311-326.
- Gauthier, P.J., Le Cloarec, M.F., Condomines, M., 2000. Degassing processes at Stromboli volcano inferred from short-lived disequilibria ( $^{210}\text{Pb}$ – $^{210}\text{Bi}$ – $^{210}\text{Po}$ ) in volcanic gases. *Journal of Volcanology and Geothermal Research*, 102(1): 1-19.
- Getahun, A., Reed, M.H., Symonds, R., 1996. Mount St. Augustine volcano fumarole wall rock alteration: mineralogy, zoning, composition and numerical models of its formation process. *Journal of Volcanology and Geothermal Research*, 71(2): 73-107.
- Gurioli, L. et al., 2018. Integrating field, textural, and geochemical monitoring to track eruption triggers and dynamics: a case study from Piton de la Fournaise. *Solid Earth*, 9(2): 431-455.
- Jenner, F.E. et al., 2015. The competing effects of sulfide saturation versus degassing on the behavior of the chalcophile elements during the differentiation of hydrous melts. *Geochemistry, Geophysics, Geosystems*, 16(5): 1490-1507.
- Jenner, F.E., O'Neill, H.S.C., Arculus, R.J., Mavrogenes, J.A., 2010. The Magnetite Crisis in the Evolution of Arc-related Magmas and the Initial Concentration of Au, Ag and Cu. *Journal of Petrology*, 51(12): 2445-2464.
- John, M.K., Saunders, W.M.H., Watkinson, J.H., 1976. Selenium adsorption by New Zealand soils. *New Zealand Journal of Agricultural Research*, 19(2): 143-151.
- Johnson, C.M., Beard, B.L., 1999. Correction of instrumentally produced mass fractionation during isotopic analysis of Fe by thermal ionization mass spectrometry. *International Journal of Mass Spectrometry*, 193(1): 87-99.
- Johnson, T.M., 2004. A review of mass-dependent fractionation of selenium isotopes and implications for other heavy stable isotopes. *Chemical Geology*, 204(3): 201-214.
- Johnson, T. M., and Bullen, T. D., 2004. Mass-dependent fractionation of selenium and chromium isotopes in low-temperature environments. In Johnson, C. M., Beard, B. L., and Albarède, F. (eds.), *Geochemistry of Non-traditional Stable Isotopes*. Washington: Mineralogical Society of America and Geochemical Society, pp. 289–317.
- Khawiwada, S., Subedi, A., 2021. A Mechanistic Link Between Selenium and Coronavirus Disease 2019 (COVID-19). *Current Nutrition Reports*, 10(2): 125-136.
- König, S., Luguet, A., Lorand, J.-P., Wombacher, F., Lissner, M., 2012. Selenium and tellurium systematics of the Earth's mantle from high precision analyses of ultra-depleted orogenic peridotites. *Geochimica et Cosmochimica Acta*, 86: 354-366.

- Kurzawa, T., König, S., Alt, J.C., Yierpan, A., Schoenberg, R., 2019. The role of subduction recycling on the selenium isotope signature of the mantle: Constraints from Mariana arc lavas. *Chemical Geology*, 513: 239-249.
- Kurzawa, T., König, S., Labidi, J., Yierpan, A., Schoenberg, R., 2017. A method for Se isotope analysis of low ng-level geological samples via double spike and hydride generation MC-ICP-MS. *Chemical Geology*, 466: 219-228.
- Labidi, J., König, S., Kurzawa, T., Yierpan, A., Schoenberg, R., 2018. The selenium isotopic variations in chondrites are mass-dependent; Implications for sulfide formation in the early solar system. *Earth and Planetary Science Letters*, 481: 212-222.
- Lambert, G., Le Cloarec, M.F., Ardouin, B., Le Roulley, J.C., 1985. Volcanic emission of radionuclides and magma dynamics. *Earth and Planetary Science Letters*, 76(1): 185-192.
- Lénat, J.-F., Gibert-Malengreau, B., Galdéano, A., 2001. A new model for the evolution of the volcanic island of Réunion (Indian Ocean). *Journal of Geophysical Research: Solid Earth*, 106(B5): 8645-8663.
- Lissner, M. et al., 2014. Selenium and tellurium systematics in MORBs from the southern Mid-Atlantic Ridge (47–50°S). *Geochimica et Cosmochimica Acta*, 144: 379-402.
- Liuzzo, M. et al., 2015. New evidence of CO<sub>2</sub> soil degassing anomalies on Piton de la Fournaise volcano and the link with volcano tectonic structures. *Geochemistry, Geophysics, Geosystems*, 16(12): 4388-4404.
- Mason, E. et al., 2021. Volatile metal emissions from volcanic degassing and lava–seawater interactions at Kīlauea Volcano, Hawai‘i. *Communications Earth & Environment*, 2(1): 79.
- Mather, T.A., Pyle, D.M., Oppenheimer, C., 2004. Tropospheric Volcanic Aerosol, *Volcanism and the Earth's Atmosphere*, pp. 189-212.
- Mosher, B.W., Duce, R.A., 1987. A global atmospheric selenium budget. *Journal of Geophysical Research: Atmospheres*, 92(D11): 13289-13298.
- Nakamaru, Y., Tagami, K., Uchida, S., 2005. Distribution coefficient of selenium in Japanese agricultural soils. *Chemosphere*, 58(10): 1347-1354.
- Nakamaru, Y., Tagami, K., Uchida, S., 2006. Effect of phosphate addition on the sorption-desorption reaction of selenium in Japanese agricultural soils. *Chemosphere*, 63(1): 109-115.
- Nakamaru, Y.M., Sekine, K., 2008. Sorption behavior of selenium and antimony in soils as a function of phosphate ion concentration. *Soil Science & Plant Nutrition*, 54(3): 332-341.
- Nriagu, J.O., 1989. A global assessment of natural sources of atmospheric trace metals. *Nature*, 338(6210): 47-49.
- Peak, D., Sparks, D.L., 2002. Mechanisms of Selenate Adsorption on Iron Oxides and Hydroxides. *Environmental Science & Technology*, 36(7): 1460-1466.
- Peltier, A., Bachèlery, P., Staudacher, T., 2009. Magma transport and storage at Piton de La Fournaise (La Réunion) between 1972 and 2007: A review of geophysical and geochemical data. *Journal of Volcanology and Geothermal Research*, 184(1): 93-108.
- Pietruszka, A.J., Hauri, E.H., Blichert-Toft, J., 2009. Crustal Contamination of Mantle-derived Magmas within Piton de la Fournaise Volcano, Réunion Island. *Journal of Petrology*, 50(4): 661-684.

- Plank, T., Kelley, K.A., Zimmer, M.M., Hauri, E.H., Wallace, P.J., 2013. Why do mafic arc magmas contain ~4wt% water on average? *Earth and Planetary Science Letters*, 364: 168-179.
- Rayman, M.P., 2000. The importance of selenium to human health. *The Lancet*, 356(9225): 233-241.
- Reekie, C.D.J. et al., 2019. Sulfide resorption during crustal ascent and degassing of oceanic plateau basalts. *Nat Commun*, 10(1): 82.
- Rodríguez-Mercado, J.J., Altamirano-Lozano, M.A., 2013. Genetic toxicology of thallium: a review. *Drug and Chemical Toxicology*, 36(3): 369-383.
- Roult, G. et al., 2012. A new comprehensive classification of the Piton de la Fournaise activity spanning the 1985–2010 period. Search and analysis of short-term precursors from a broad-band seismological station. *Journal of Volcanology and Geothermal Research*, 241-242: 78-104.
- Servadio, Z., 2011. Apports de l'imagerie à haute résolution spectrale et spatiale dans le sbilans de volume et bilans radiatifs au Piton de La Fournaise, Université de la Réunion.
- Schauble, E.A., 2004. Applying stable isotope fractionation theory to new systems. *Reviews in Mineralogy and Geochemistry* 55, 65-111.
- Shannon, R.D., 1976. Revised effective ionic radii and systematic studies of interatomic distances in halides and chalcogenides. *Acta Crystallographica Section A*, 32(5): 751-767.
- Silva, T.P. et al., 2019. Mineralogy and chemistry of incrustations resulting from the 2014–2015 eruption of Fogo volcano, Cape Verde. *Bulletin of Volcanology*, 81(4): 23.
- Small, C., Naumann, T., 2001. The global distribution of human population and recent volcanism. *Global Environmental Change Part B: Environmental Hazards*, 3(3): 93-109.
- Staudacher, T. et al., 2009. The April 2007 eruption and the Dolomieu crater collapse, two major events at Piton de la Fournaise (La Réunion Island, Indian Ocean). *Journal of Volcanology and Geothermal Research*, 184(1): 126-137.
- Stoiber, R.E., Rose, W.I., 1974. Fumarole incrustations at active central american volcanoes. *Geochimica et Cosmochimica Acta*, 38(4): 495-516.
- Sunde, R.A., 2012. Selenium. *Modern nutrition in health and disease*. Lippincott Williams & Wilkins, Philadelphia, PA.
- Tetsuro, S., 1964. A Geochemical Study of Selenium in Volcanic Exhalation and Sulfur Deposits. *Bulletin of the Chemical Society of Japan*, 37(8): 1200-1206.
- Toutain, J.P. et al., 1990. Vapor deposition of trace elements from degassed basaltic lava, Piton de la Fournaise volcano, Reunion Island. *Journal of Volcanology and Geothermal Research*, 40(3): 257-268.
- Toutain, J.P. et al., 2003. A new collector for sampling volcanic aerosols. *Journal of Volcanology and Geothermal Research*, 123(1): 95-103.
- Toutain, J.P. et al., 2008. Evidence for Zn isotopic fractionation at Merapi volcano. *Chemical Geology*, 253(1): 47 - 82.
- Varas-Reus, M.I., König, S., Yierpan, A., Lorand, J.-P., Schoenberg, R., 2019. Selenium isotopes as tracers of a late volatile contribution to Earth from the outer Solar System. *Nature Geoscience*, 12(9): 779-782.
- Vlastélic, I. et al., 2009. Pb isotope geochemistry of Piton de la Fournaise historical lavas. *Journal of Volcanology and Geothermal Research*, 184(1): 63-78.

- Vlastélic, I. et al., 2013. Lead isotopes behavior in the fumarolic environment of the Piton de la Fournaise volcano (Réunion Island). *Geochimica et Cosmochimica Acta*, 100: 297-314.
- Wasserman, N.L., Schilling, K., Johnson, T.M., Pallud, C., 2021. Selenium Isotope Shifts during the Oxidation of Selenide-Bearing Minerals. *ACS Earth and Space Chemistry*, 5(5): 1140-1149.
- Wen, H., Carignan, J., 2007. Reviews on atmospheric selenium: Emissions, speciation and fate. *Atmospheric Environment*, 41(34): 7151-7165.
- Wieser, P.E., Jenner, F., Edmonds, M., MacLennan, J., Kunz, B.E., 2020. Chalcophile elements track the fate of sulfur at Kīlauea Volcano, Hawai'i. *Geochimica et Cosmochimica Acta*, 282: 245-275.
- Wijnja, H., Schulthess, C.P., 2000. Vibrational Spectroscopy Study of Selenate and Sulfate Adsorption Mechanisms on Fe and Al (Hydr)oxide Surfaces. *Journal of Colloid and Interface Science*, 229(1): 286-297.
- Wood, B.J., Smythe, D.J., Harrison, T., 2019. The condensation temperatures of the elements: A reappraisal. *American Mineralogist*, 104(6): 844-856.
- Wu, C.-H., Lo, S.-L., Lin, C.-F., 2000. Competitive adsorption of molybdate, chromate, sulfate, selenate, and selenite on  $\gamma$ -Al<sub>2</sub>O<sub>3</sub>. *Colloids and Surfaces A: Physicochemical and Engineering Aspects*, 166(1): 251-259.
- Yierpan, A. et al., 2018. Chemical Sample Processing for Combined Selenium Isotope and Selenium-Tellurium Elemental Investigation of the Earth's Igneous Reservoirs. *Geochemistry, Geophysics, Geosystems*, 19(2): 516-533.
- Yierpan, A., König, S., Labidi, J., Schoenberg, R., 2019. Selenium isotope and S-Se-Te elemental systematics along the Pacific-Antarctic ridge: Role of mantle processes. *Geochimica et Cosmochimica Acta*, 249: 199-224.
- Yierpan, A., König, S., Labidi, J., Schoenberg, R., 2020. Recycled selenium in hot spot-influenced lavas records ocean-atmosphere oxygenation. *Science Advances*, 6(39): eabb6179.
- Yierpan, A., Redlinger, J., König, S., 2021. Selenium and tellurium in Reykjanes Ridge and Icelandic basalts: Evidence for degassing-induced Se isotope fractionation. *Geochimica et Cosmochimica Acta*.
- Zelenski, M., Simakin, A., Taran, Y., Kamenetsky, V.S., Malik, N., 2021. Partitioning of elements between high-temperature, low-density aqueous fluid and silicate melt as derived from volcanic gas geochemistry. *Geochimica et Cosmochimica Acta*, 295: 112-134.

**Table 1.** Characteristics and geochemical data of the lavas, fumarolic deposits and rock reference materials analyzed in this study

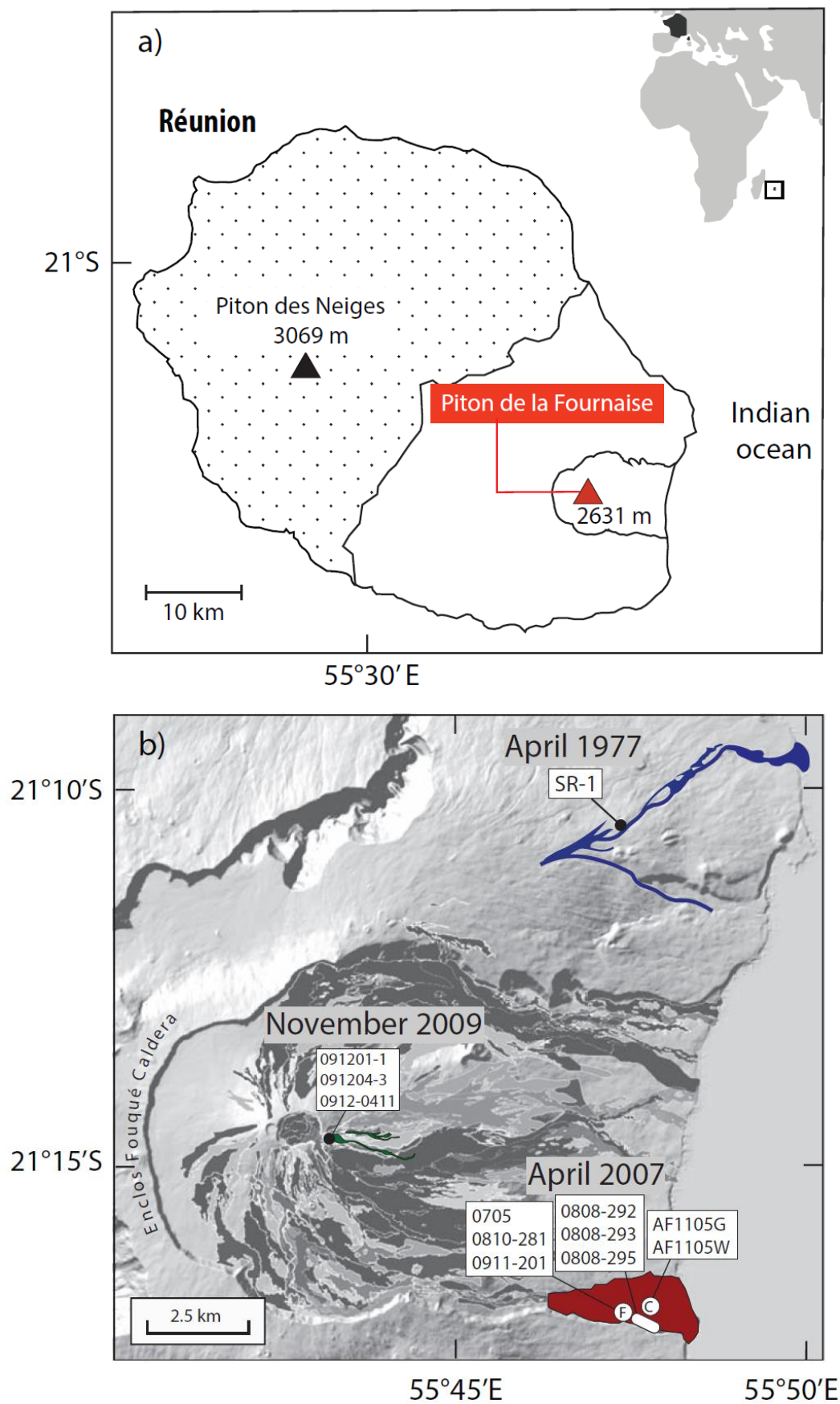
Eruption year	Sample date	Sample name	Coordinates		Material	Formation or condensation Temp. (°C)	Se	Te	$\delta^{82/76}\text{Se}$	2 s.e.	Be	EF <sub>Se/Be</sub>	MgO (wt.%)	Se olivine-corrected*
			Lat. (S)	Long. (E)			(ng/g)	(ng/g)	(‰)	(‰)	(ng/g)			
<b>LAVAS</b>														
2007	2007/04	REU 0704-04	21°17'24"	55°47'49"	Basaltic lava	1185	136	0.299	0.12	0.05	930	1.0	7.3	135
2007	2007/04	REU 0704-05-1	21°17'24"	55°47'49"	Basaltic lava	1185	72	0.129	0.04	0.06	570	0.87	21	124
2007	2007/04	REU 0704-08-1	21°17'24"	55°47'49"	Basaltic lava	1185	58	0.252	0.23	0.15	400	1.0	29.2	142
2009	2009/11	REU 0912-01-1	21°14'45.3"	55°43'15.6"	Basaltic lava	1155	94	0.115	0.06	0.07	1030	0.63	7.8	96
2009	2009/11	REU 0912-04-3	21°14'45.3"	55°43'15.6"	Basaltic glass	1155	138	0.277	-0.19	0.04	1050	0.90	8.3	141
<b>FUMAROLIC DEPOSITS</b>														
2009	2009/11	REU 0912-0411	21°14'45.3"	55°43'15.6"	Thenardite	800	1698	82	-0.44	0.04	32	363		
2007	2008/06	REU 0705	21°17'14.8"	55°47'34"	Na-K sulfate	400	1552	453	-0.91	0.04	2760	3.8		
2007	2008/10	REU 0810-281a	21°17'14.8"	55°47'34"	Na-K sulfate	384	807	285	-0.94	0.07	2200	2.5		
2007	2008/10	REU 0810-281b	21°17'14.8"	55°47'34"	Na-K sulfate	384	849	332	-1.03	0.04	2200	2.6		
2007	2009/11	REU 0911-201	21°17'14.8"	55°47'34"	Na-K sulfate	325	543	589	-1.46	0.15	2040	1.8		
2007	2010	AF 1105 G	21°17'17.1"	55°47'46.2"	Gypsum/Cu sulfate	200	2686	1.631	-1.37	0.06	209	88		
2007	2011/05	AF 1105Wa	21°17'17.1"	55°47'46.2"	Gypsum	120	2577	0.437	-1.94	0.12	114	155		
2007	2011/05	AF 1105Wb	21°17'17.1"	55°47'46.2"	Gypsum	120	11298	0.437	-2.08	0.06	114	679		
2007	2008/08	REU 0808-292a	21°17'17.5"	55°47'41.2"	Thenardite	100 <sup>‡</sup>	13617	0.257	-0.97	0.05	140	666		
2007	2008/08	REU 0808-293a	21°17'19.7"	55°47'45.8"	Ca-Mg-Al-Fe fluorides	100	119797	7.79	-0.85	0.03	550	1491		
2007	2008/08	REU 0808-293b	21°17'19.7"	55°47'45.8"	Ca-Mg-Al-Fe fluorides	100	118953	7.79	-0.83	0.04	550	1481		
2007	2008/08	REU 0808-293c	21°17'19.7"	55°47'45.8"	Ca-Mg-Al-Fe fluorides	100	370147	7.79	-0.94	0.07	550	4608		
2007	2008/08	REU 0808-295	21°17'19.8"	55°47'46.1"	Ca-Mg-Al-Fe fluorides	100	82322	0.1	-0.55	0.07	420	1342		
1977	1977/04	SR-1a	21°10'48"	55°46'48"	Native sulfur	100	1.571 x 10 <sup>6</sup>		0.65	0.08	< 5	> 2 x 10 <sup>6</sup>		
1977	1977/04	SR-1b	21°10'48"	55°46'48"	Native sulfur	100	1.584 x 10 <sup>6</sup>		0.55	0.05	< 5	> 2 x 10 <sup>6</sup>		
<b>ROCK REFERENCE MATERIALS</b>														
		BCR-2 a			Basaltic lava		80	2.7	0.08	0.07				
		BCR-2 b			Basaltic lava		78	2.8	0.12	0.13				
		BCR-2 c			Basaltic lava		78	2.3	0.16	0.04				
		W-2a			Diabase		103	1.8	-0.09	0.07				

\*Se (at MgO: 7.5 wt. %) = Se - S · (MgO - 7.5) where S is the slope of the Se vs. MgO correlation in the lavas (S = - 3.863), and assuming an initial Se content of 200 ng·g<sup>-1</sup> (Collins et al., 2012), as well as an initial  $\delta^{82/76}\text{Se}$  of -0.30 ‰.

The data presented for native sulfur (SR-1a, and SR-1b) are two replicates based on individual digests.

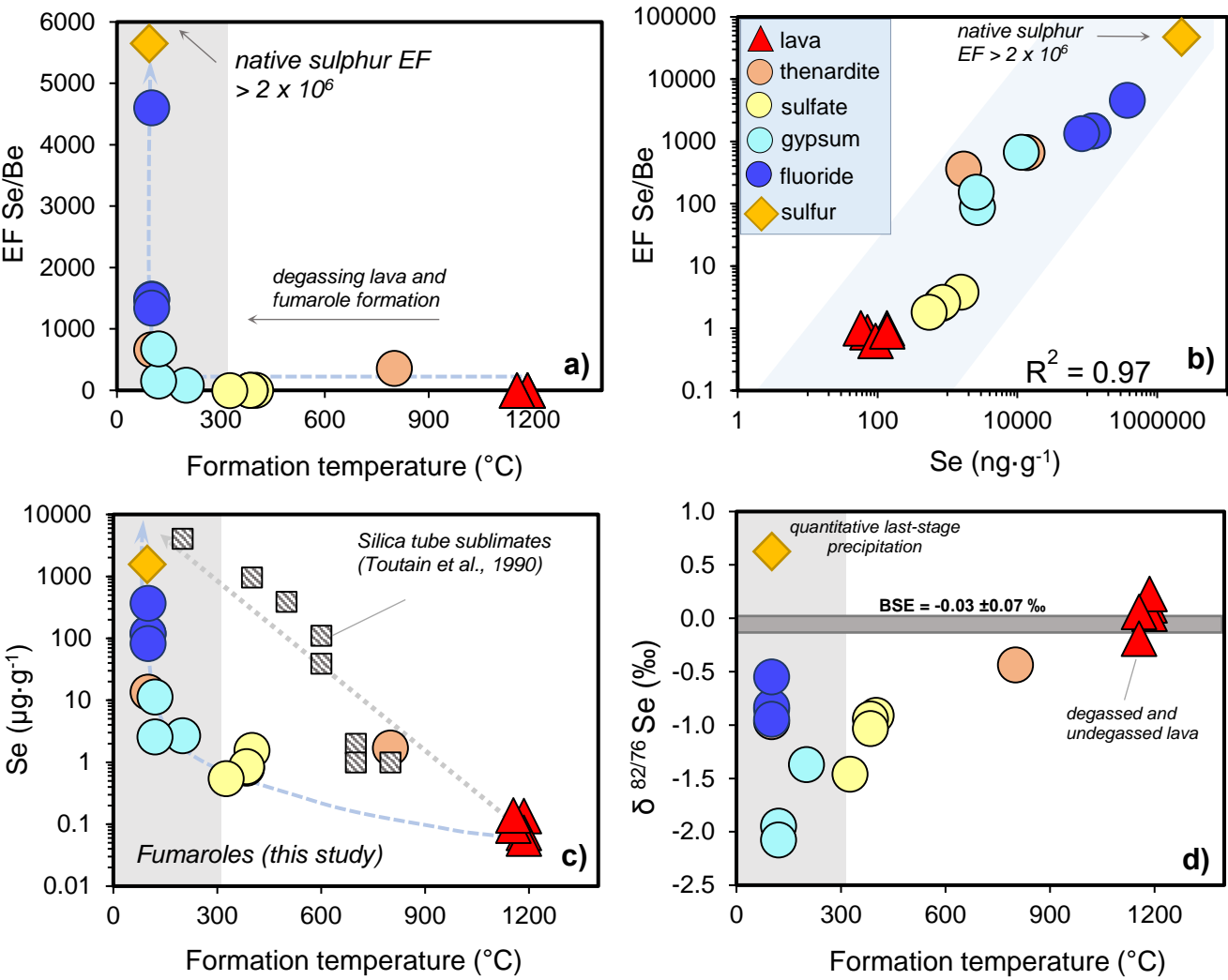
<sup>‡</sup> Thenardite initially formed at higher temperature but then dissolved in aqueous solution and reprecipitated at ca. 100°C.

Rosca et al. Fig. 1

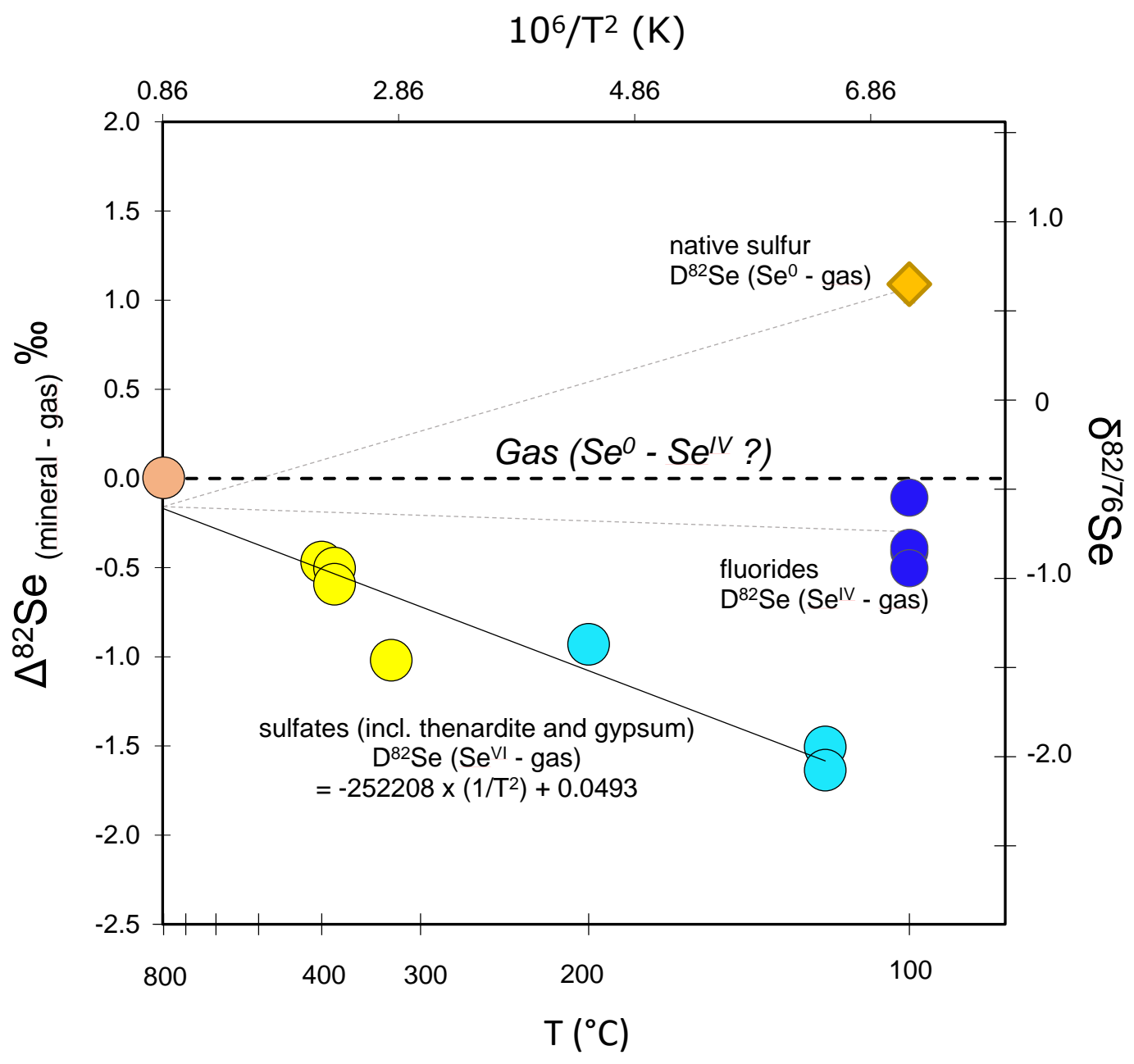




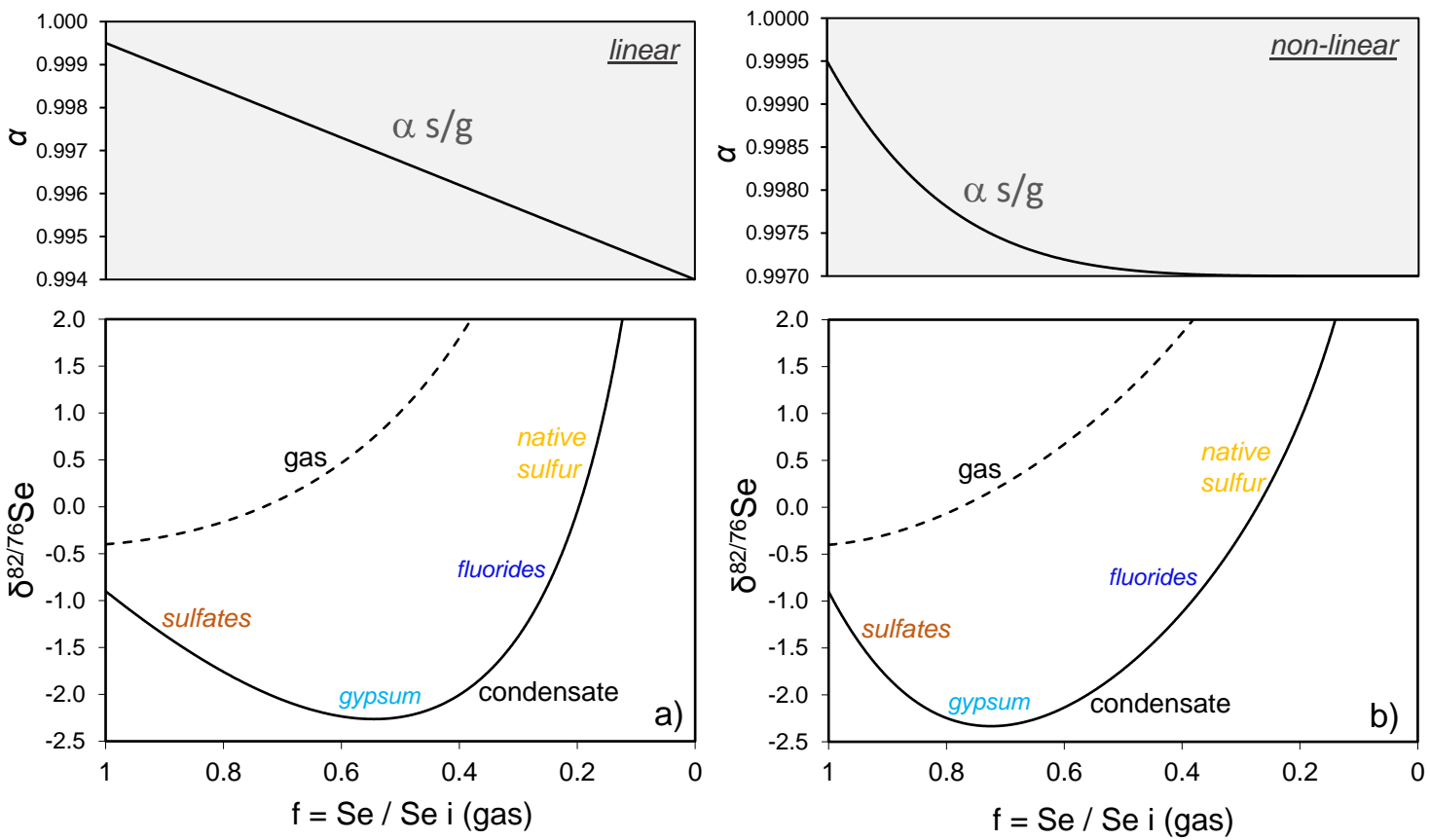
Rosca et al. Fig. 2



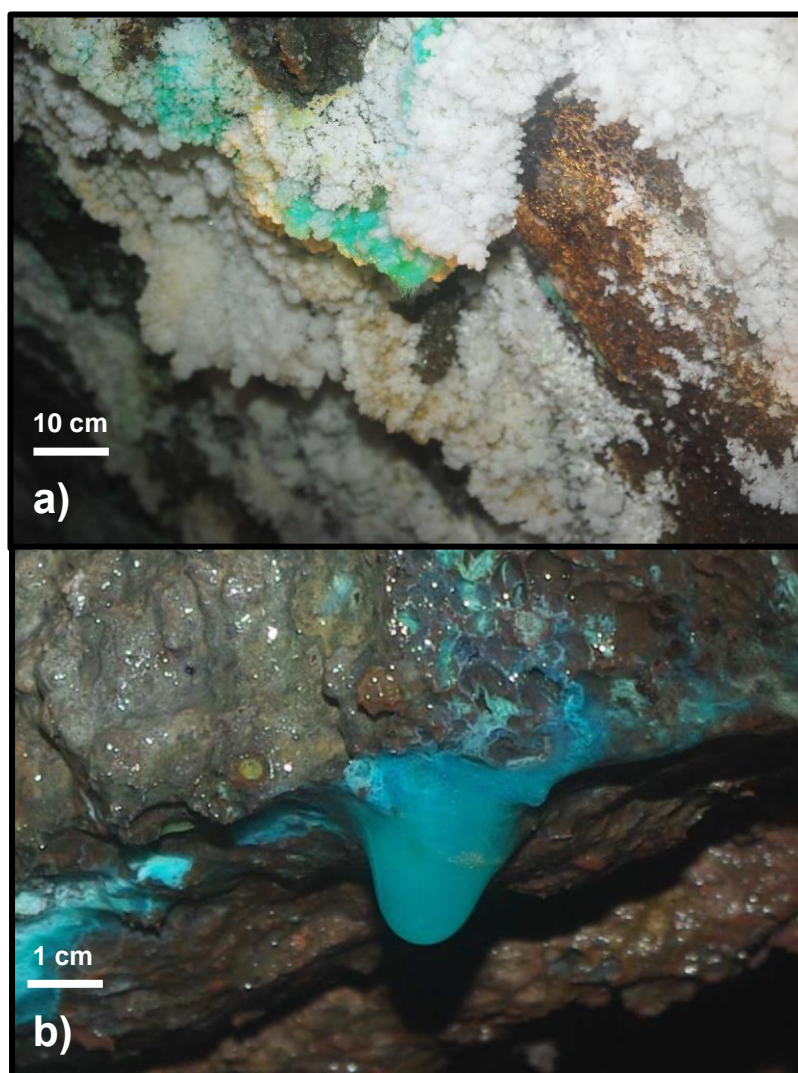
Rosca et al. Fig. 3



Rosca et al. Fig. 4



Rosca et al. Fig. 5



Rosca et al. Fig. 6

